Innovative Sand Groin Beach Nourishment with Environmental, Protection and Recreational Purposes

Piero Ruol, Luca Martinelli, Chiara Favaretto, Daniele Scroccaro
ICEA Department, University of Padova
Padova, Italy

ABSTRACT

This paper presents a 3D experimental-investigation (in scale 1 to 50) carried out to reproduce the short-term evolution of beach nourishment with two equally sized (15,000 m^3) but differently shaped disposals: 1) two sandy groins, representing localized nourishments and 2) a distributed nourishment. The aims are to investigate the short-term planform and profile evolution for the two cases, under the wave forcing of typical Adriatic Sea (Italy) storms and to compare the experimental results with a 2DH numerical model (XBeach). The "sand groins" nourishment, which is needed to mitigate erosion, evolved into a dune-lagoon system that makes the environment more attractive and is an appealing prospect for tourism.

KEY WORDS: sand groin, nourishment, XBeach, wave basin

INTRODUCTION

Dean (2002) considers plain nourishment as a preferential remedy for coastal erosion and flooding. Suitable sand is usually placed along a certain stretch of the coast, shifting the mean water line seaward. In order to reduce placement costs, the same amount of sand may be dumped in concentrated areas, thus relying on the natural nearshore sediment transport processes to redistribute the nourishment along the adjoining sections of the coast.

A well-documented example of local nourishment is the Netherlands' "Sand Engine" project (Stive et al., 2013), in which a huge, highly concentrated volume of sand (17 Mm^3) was placed in the shape of a large peninsula (named, in fact, "Sand Engine peninsula") that protruded 1 km from shore. The objective was to provide safety against flooding and create new spatial values.

Shoreline evolution after distributed or localized nourishment can be predicted by numerical models such as XBeach, developed by Roelvink et al. (2009). The XBeach model has been shown to perform well in 2D laboratory tests in cases of retreating beaches (Roelvink et al., 2009; Van Thiel de Vries., 2009). Simulations of 2D wave run-ups and inundations (McCall et al., 2010) suggest that the model is capable of reproducing the 2D morphological features common to overwash, such as foredune erosion, back barrier deposition and washover fans. There is also an avalanching mechanism that helps to predict dune undercutting (van Gent et al., 2008) in saturated and dry sand.

Recently, XBeach has compared successfully with prototype observation of dune erosion (de Winter et al. 2015) and barrier-island breaching (Williams et al., 2015). For instance, Harter & Figlus (2017) modelled, with XBeach, the impact of the Hurricane Ike on the subaerial morphology of a stretch of coastline along the Gulf of Mexico, comparing results with another numerical model CSHORE (Kobayashi, 2016). Despite computationally less efficient, XBeach resulted more accurate at simulating the coastal response and able to capture 2D effects such as the locations of large breaches.

The morphological processes related to short-term evolution of beach nourishment is, however, very complex to study in real conditions, due to the inherent uncertainty of actual constraints and to the complexity of the environment examined. Several experimental studies on short-term post-nourishment regression and sediment transport rates are available for 2D conditions and, an overview of work on beach nourishment in large wave flumes was given by Dette et al. (2002). More recently, Di Risio et al. (2010) carried out a wave flume experimental investigation in order to reproduce the cross-shore evolution of unprotected sandy beaches and ones protected by submerged breakwaters. Grasso et al. (2011) studied the morphological response of nourishment placed either on the outer bar or directly on the beach face. Ruessink et al. (2016) used a large scale laboratory to investigate cross-shore sediment transport under "erosive" storm waves and "accretive" swell waves.

Scale effects were studied within the EU-SANDS Project in which three wave flumes with different geometrical scales were used to reproduce identical wave conditions (Grüne et al., 2008).

Experiments in 3D conditions, i.e. carried out in wave basins, focusing on the evolution of traditional distributed nourishments. For instance, Work and Rogers (1998) investigated in a wave basin the influence of several wave and beach parameters on the rate of diffusion from a nourished beach, involving two different nourishment planforms. Karasu et al. (2008) conducted a series of 3D laboratory experiments on

beach nourishment behavior in order to analyze the influences of berm height, beachfill median grain size, wave height, and wave period. Martinelli et al. (2006) described beach evolution protected by submerged barriers. Ruol et al. (1997) and Tondello et al. (1998) used a wave basin to investigate the reshaping of beach nourishment based on a large number (39) of sand groins that were to be remodelled by wave action.

In conclusion, the experimental studies available provide sufficient information to calibrate the numerical models for distributed nourishments, but further investigation is necessary for localized ones.

In view of possible applications along Northern Italy's Adriatic coast, experimental and numerical investigations were carried out in order to examine the evolution of two different types of small localized maintenance nourishment under the wave forcing of typical Italian storms.

This paper compares the traditional configuration of a rectangular-shaped nourishment with an innovative design called "sand groins". Actually, the geometry of the two configurations was not optimized but fits with local constraints and available resources in the hypothesis of distribution with dumpers just before the tourist season.

From a technical point of view, the second design may be the easiest to build up because the volume of sediment is concentrated in some specific points along the coast. The impact associated with the building phase of this layout is evidently much lower than traditional nourishment since shoreline disturbance is minimal, as is the interference of works with beach use.

This paper is organized as follows: the next section describes the experimental tests. The experimental results for the two nourishment configurations are then presented separately. A subsequent chapter presents calibration and discusses the results of the XBeach numerical model. Finally, the conclusions are drawn. An annex presents the details of the numerical calibration procedure.

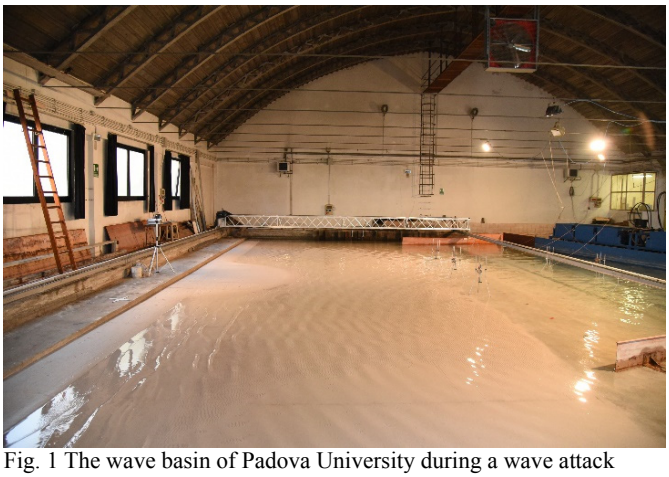

Fig. 1 The wave basin of Padova University during a wave attack

PHYSICAL MODEL TEST

The experimental investigation was performed in the University of Padova wave basin, which is 20.6 m × 17.8 m × 0.8 m (Fig. 1). The wave-maker is 12 m wide and can generate irregular long-crested waves.

The sand used for the movable bed is industrial quartz sand processed to have a very narrow fuse, which ranges from 0.06 to 0.2 mm (ρ_s = 2600 kg/m^3) with d_{50} = 0.15 mm (Fig. 2).

The movable bed model was built in scale $\lambda = 1{:}50$ and a Froude similarity ($\lambda_T = \lambda^{1/2}$) was used to scale down time. Therefore, the tested grain size is approximately equal to 0.42 mm in prototype scale (using the Dean similarity, i.e. fall velocity in Froude similarity), slightly outside the typical range of sand of the Northern Adriatic Sea (Ruol et al., 2018), but still realistic.

The un-nourished initial bed profile was uniform along the shore and characterized in the cross-shore direction by two slopes, in the nearshore and offshore zones: the slope is 0.025 shoreward of the 2.6 m isobath (5.2 cm at model scale) and 0.01 offshore of this isobath. The water depth at the wavemaker was 20.6 m (41.1 cm at model scale).

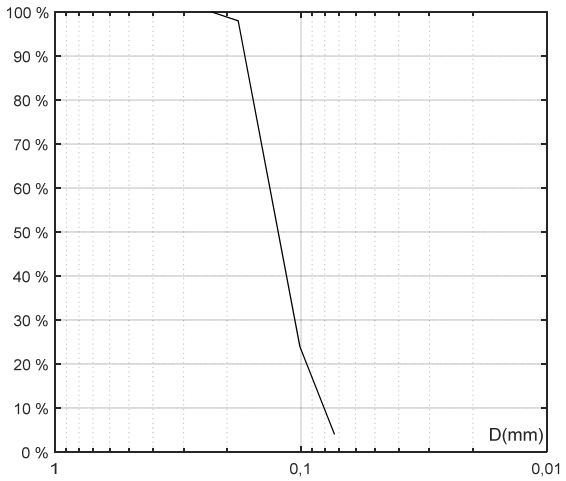

Fig. 2 Grain size distribution curve of the quartz sand (d_{50} = 0.15 mm)

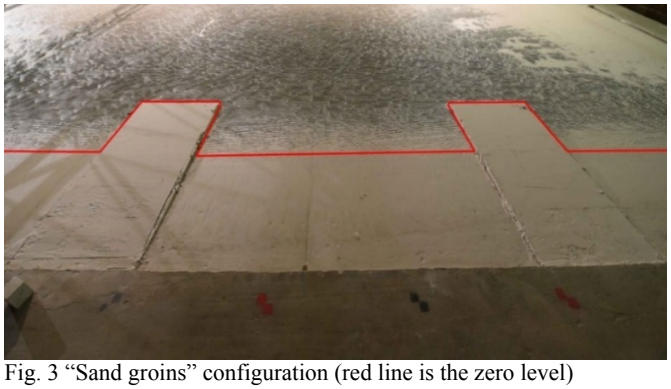

Fig. 3 "Sand groins" configuration (red line is the zero level)

Fig. 4 Traditional nourishment configuration (red line is the zero level)

In order to obtain a realistic and natural un-nourished shape, the beach was subjected to an oblique (15°) wave attack formed by three irregular sea states: 1) Hs=3 cm, T=1 s, 10 min; 2) Hs=5 cm, T=1.2 s, 10 min;

and 3) Hs=3 cm, T=1 s, 10 min (in model scale). Two guidewalls were placed at both sides of the wavemaker to minimize the effect of diffraction.
After this phase, the first nourishment configuration consisting of two sand groins was built. (Fig. 3, Fig. 5 left, nourished volume ~15,000 m^3 in prototype scale).
After the sand groins had been tested, the initial bed was remodelled and the same procedure as the first case was used to build the second configuration, which comprised ~15,000 m^3 of localized nourishment (Fig. 4, Fig. 5 right). Tab. 1 and Tab. 2 show the geometry of the configurations investigated.

Tab. 1 Sand groins

Scale	groin width (m)	length (m)	height (m)	distance between groins (m)	Vol. (m^3)
Prototype	50	96	1.50	200	14'803
Model	1.00	1.91	0.03	4	0.12

Tab. 2 Traditional nourishment

Scale	nourishment length (m)	stretch of coast (m)	height (m)	Vol. (m^3)
Prototype	62.5	300	1.15	14'803
Model	1.25	6	0.023	0.12

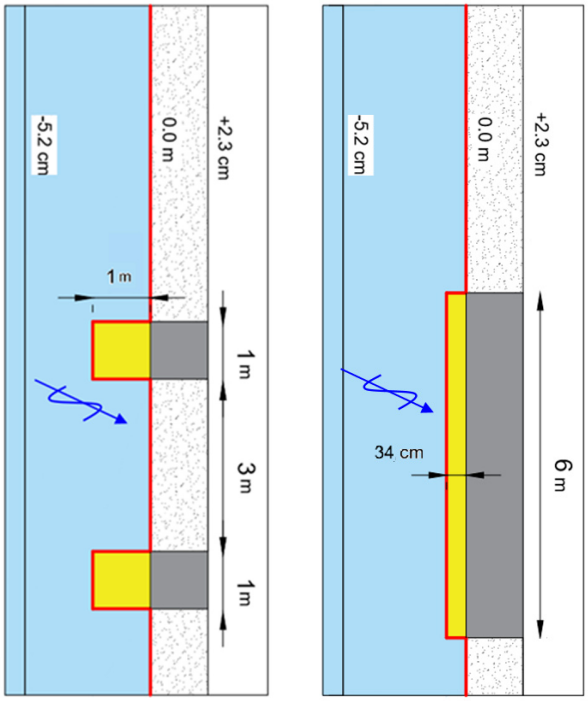

Fig. 5 Scheme of the "sand groins" configuration (left), scheme of the traditional nourishment configuration (right)

For each configuration, a "typical" storm with 15° obliquity was repeated three times consecutively. The irregular long-crested waves were generated according to a JONSWAP spectrum (γ = 3.3). The simulated storm is the schematization of a real one (Fig. 6); it has a return period of 1 year and was recorded on 01/12/2008 at the "CNR Platform" located on 16 m of water depth in the Northern Adriatic Sea. The characteristics of the storm used for the experimental investigation are reported in Tab. 3. The schematised storm has the same energy as the real one (wave energy ~ 110 m^2/hour). The main features of the real sea states, that were not examined but may have some influence on the longshore sediment distribution, are: wave multi-directionality, currents generated by tide, pressure or wind, randomness of the wave sequence. The wave characteristics generated were recorded by means of eight resistive wave gauges: four were placed in front of the wave generator and four were fixed to a mobile framework. The bed was levelled by means of an automatic profiler located on the mobile framework. The profiler can measure the bottom level in the presence of water and the submerged distance seems "shorter" by a factor equal to the ratio between the speed of light in air and in water (=1.33). Therefore, these "wet" seabed profiles were corrected by taking into account the different refraction coefficients between air and water. The bathymetry was levelled at least four times during the storm: at the beginning of the test and at the end of each sea state during the storm.

Tab. 3 Wave characteristics of the storm (repeated 3 times)

Sea state	Prototype scale			Model scale (1:50)		
	t (hours)	Hs (m)	Tp (s)	t (hours)	Hs (cm)	Tp (s)
1	7.07	1.5	7.0	1.0	3.0	1.0
2	10.66	2.5	8.8	1.5	5.0	1.2
3	14.14	1.5	7.0	2.0	3.0	1.0

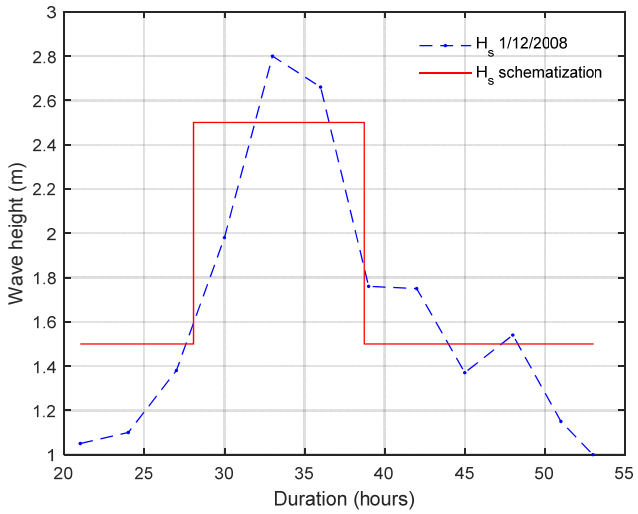

Fig. 6 Storm registered in the CNR tower on 1/12/2008 and assumed wave height schematization

KEY EXPERIMENTAL RESULTS

For the sake of brevity, this section presents the key experimental results only. Note that: i) the incident waves measured were consistent with the target ones, as a result of spectral and time domain analyses of the wave elevations; ii) the bed evolved gradually during each storm, progressing monotonically toward the final bathymetry, thus the initial and final bed surveys are sufficient for describing the entire storm evolution process. The automatic bed profiler readings were scaled at prototype dimension. Therefore Fig. 7 and Fig. 9 show the initial bathymetry of the modelled configurations at full scale, with the 12 m wavemaker scaling up to 600 m, with midpoint placed in x = 650 m and y = -300 m, orientation 15°. Since the initial bathymetry was obtained after running several waves, to recreate a natural profile more realistically, the isobaths in both configurations were irregular and not exactly straight. For completeness, all the surveyed area is shown in the figures. However, due to the presence of the guidewalls, only a portion of this area (i.e. from x = 200 m and x = 700 m) can be considered well represented and used both for calibration, analysis and to draw conclusion.

Sand groins

Fig. 8 shows the bathymetry for the "sand groins" configuration after the storm had been repeated three times. It clearly shows that the nourished sand was re-distributed downstream by the combined effect of waves and induced currents.
After the tests, the shoreline rotated to sit at more or less a right angle to the direction of the waves. Deposition and erosion, induced by circulations, caused the formation of a berm at the sand groin heads.

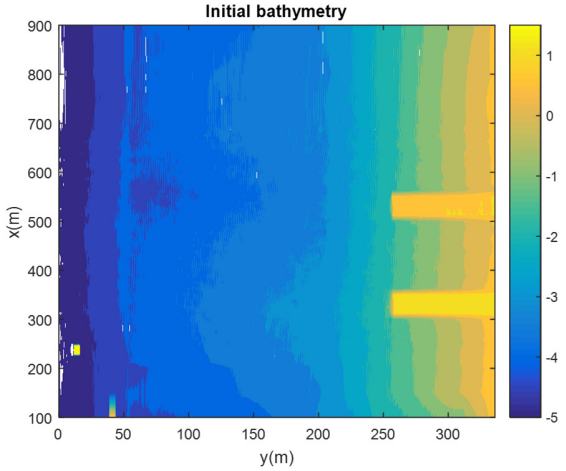

Fig. 7 Sand Groins: initial bathymetry (physical model)

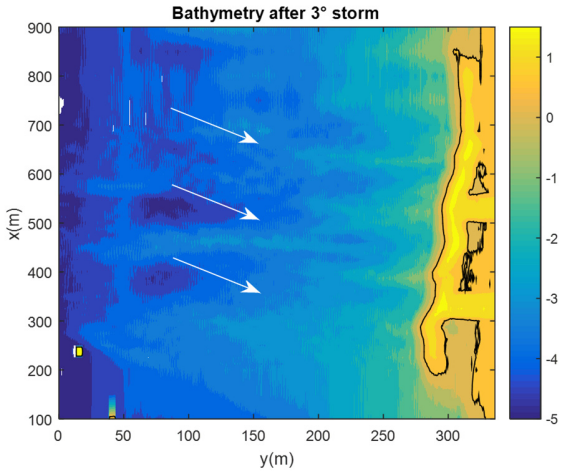

Fig. 8 Sand Groins: final bathymetry (physical model)

In presence of the groins the current intensity is reasonably reduced close to the shore and enhanced close to the groin heads (as confirmed by numerical simulations), and the consequences are observed in the erosive and accretive pattern. The evolution of the emerged and submerged beach at the end of the tests revealed the formation of a small dune-lagoon system, suitable for environmental purposes, such as biodiversity conservation or "green" tourism.

Traditional Nourishment

Fig. 10 shows the bed after the "traditional nourishment" configuration tests. As in the previous case, the shoreline rotated to form almost a right angle with the incident wave. It was also observed that the initial rectangular geometry of the shoreline remained unaltered for a longer period, i.e. no large deformation was observed after the first storm.

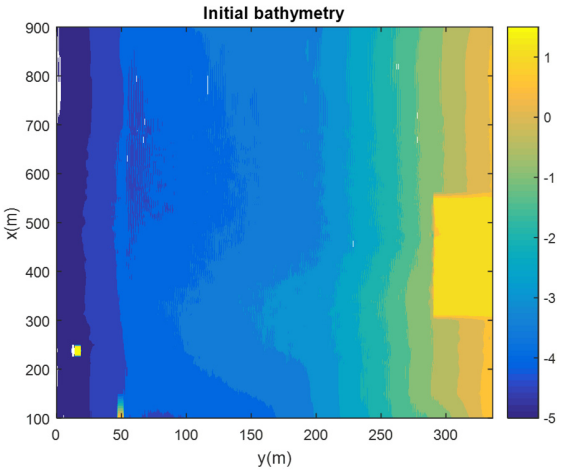

Fig. 9 Traditional nourishment: initial bathymetry (physical model)

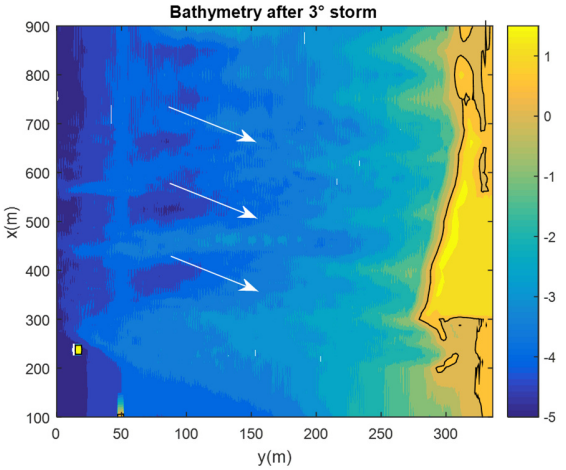

Fig. 10 Traditional nourishment: final bathymetry (physical model)

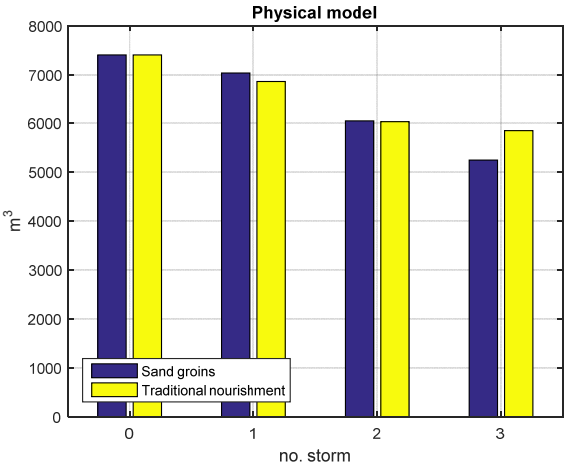

Fig. 11 Evolution of the volume of sand relative to the updrift half of the nourishment

The combined effect of wave and current produced some vorticity up-drift and down-drift the nourished beach, inducing the motion of sediments along the shoreline caused by a cross-shore transport.
Fig. 11 shows the sand volume in the area where the updrift part of the nourishment was placed (i.e. half of the total volume, 7400 m^3). The first bar represents the initial nourished volume in such area and the

following ones show its evolution after each storm.
For the traditional configuration, the sand was observed to move downdrift at a rather constant rate of 500 m^3/storm. For the sand-groin case, the dynamics is more complex and not constant and, after three storms, the volume that appears "lost" (shifted downdrift) is larger.

NUMERICAL MODEL

The numerical model used for the analysis is XBeach, a public-domain model that has been developed with funding and support by the US Army Corps of Engineers and by a consortium of UNESCO-IHE, Deltares (Delft Hydraulics), Delft University of Technology and the University of Miami, Roelvink et al. (2009).
The hydrostatic Nonlinear Shallow Water Equations are solved, decoupled from: i) the wave field, obtained by a wave action balance that uses the Janssen & Battjes (2007) model for wave breaking; ii) the morphological module, obtained by the Advection Diffusion Equation and the Soulsby-Van Rijn formulation (Van Rijn, 1984; Soulsby, 1997), for sediment transport. The bed was updated every 10 steps of hydrodynamic computation. The implementation was at full scale (50 times larger than the physical model).

Tab. 4 Configuration adopted in the Sand groins simulations, with reference to the variable names used by XBeach software

morphology	1	**alpha**	1
avalanching	1	**roller**	1
sedtrans	1	**wetslp**	0.055
bdslpeffmag	soulsby_bed	**facsl**	1.6
sourcesink	0	**rhos**	2600
ne_layer	-	**struct**	1
single_dir	1	**dzg1**	1
morstart	0	**facua**	0.2
bcfile	-	**front**	abs_2d
thetamin	330	**tstart**	0
thetamax	360	**tstop**	34416
outputformat	-	**tintg**	120
instat	40	**break**	janssen
beta	0.06	**gamma**	0.78
dryslp	1	**C**	32
form	1	**tsfac**	0.089
rho	1000	**z0**	0.02
D50	0.00042	**nd**	3
dzg2	1	**dzg3**	1
hswitch	0.55	**morfac**	10
back	abs_2d	**posdwn**	-1
zs0	0	**dtheta_s**	10
dzmax	0.03	**CFL**	0.7
tintm	120	**-**	-

The model was initialized with the bathymetries levelled in the experimental phase, as shown in Fig. 9 and Fig. 11. The model boundary conditions for the waves were as follow: in the offshore side (y = 0 m), the sequence of irregular waves listed in Table 3; at the lateral sides (x = 150 m and x = 900 m), uniform propagation; at the shoreline, absorbing condition. For the currents and levels, the boundary conditions were: in the offshore side, normal velocity and set up equal to 0; at the lateral sides, zero normal flux velocity and zero longshore gradient of the set up; at the shoreline, wet and dry algorithm.
The model was used to evaluate the morphological changes of the bed. Changes were then elaborated to find the total volume accreted/eroded along the cross-shore direction. This integral value was used to quantitatively compare the experimental to the numerical results for calibration purposes.
Tab. 4 and Tab. 5 present the values of each variable for the two configurations after the calibration procedure; the variables are listed with the name used in the software to simplify reference (http://xbeach.readthedocs.io).

Tab. 5 Configuration adopted in the Traditional nourishment case, with reference to the variable names used by XBeach software

morphology	1	**alpha**	1
avalanching	1	**roller**	1
sedtrans	1	**wetslp**	0.06
bdslpeffmag	soulsby_bed	**facsl**	1.6
sourcesink	0	**rhos**	2600
ne_layer	-	**struct**	1
single_dir	1	**dzg1**	1
morstart	0	**facua**	0.2
bcfile	-	**front**	abs_2d
thetamin	330	**tstart**	0
thetamax	360	**tstop**	34416
outputformat	-	**tintg**	120
instat	40	**break**	janssen
beta	0.095	**gamma**	0.78
dryslp	1	**C**	32
form	1	**tsfac**	0.089
rho	1000	**z0**	0.015
D50	0.0004	**nd**	3
dzg2	1	**dzg3**	1
hswitch	0.55	**morfac**	10
back	abs_2d	**posdwn**	-1
zs0	0	**dtheta_s**	10
dzmax	0.05	**CFL**	0.7
tintm	120	**-**	-

A preliminary phase of the calibration was carried out analysing the sensitivity of 9 parameters (all those that can reasonably be tuned) on the model results. The 5 that affected more significantly the results were: *beta* (breaker slope coefficient in roller model), *wetslp* (critical avalanching slope under water), *z0* (zero flow velocity level in Soulsby and van Rijn sediment concentration), *hswitch* (water depth at which wetslp switches to dryslp), *dzmax* (maximum bed-level change due to avalanching, modified only for the "sand groins" configuration) and *tsfac* (coefficient for the sediment source term, modified only for the distributed nourishment configuration). The 3 parameters that were found to less affect the results were: *alpha* (wave dissipation coefficient in Janssen formulation), *facua* (factor describing the influence of wave skewness and asymmetry on sediment transport direction), *smax* (maximum value of the Shields parameter for equilibrium sediment concentration in Van Thiel-Van Rijn formulation). The *facua* parameter is considered to have a large effect on the shoreface slope (Dissanayake et al., 2015). However, Simmons et al. (2019) show that for their case even after calibration XBeach flattened too much the beach profile in the intertidal zone. Consequently, we did not focus on the shape of the cross-shore profile, but rather on the overall accretion/erosion along the shore face. As expected, the *facua* parameter had a marginal relevance in our case. For brevity, only the second phase of the calibration procedure is documented in the Annex. Each of the 5 relevant variables was modified within a predefined range, starting from the most sensitive one. The optimal variable value chosen was the one that

provided the maximum Nash-Sutcliffe Efficiency (*NSE*) index, estimated comparing the total volume accreted/eroded along the cross-shore direction of the experimental and numerical results. Since three results were available (after the first, second and third storm) the highest average of the three *NSE* was considered. The Wilmot index *D* was also used for comparison, with it essentially providing the same result. The procedure then continued in order of sensitivity.

Fig. 12 and Fig. 13 show the results in terms of final bathymetry. The white arrows show the incident wave direction and the dotted white lines point out the shoreline re-orientation at the groin head and at the up-drift corner of the distributed nourishment. In the case of the sand groins, the down-drift groin was longer than the up-drift one at the end of the simulation. These two key elements accurately reflect the experimental findings shown in Fig. 8 and Fig. 10. Note that the observed and simulated shoreline orientation (dotted white line) was not caused by a lateral constraint. This feature is difficult to interpret numerically. A typical diffusive 1D numerical model does not predict rotation in accordance with the incident wave direction (in absence of lateral constraints) thus shoreline evolution is the same when the obliquity of the incident wave is positive or negative (Dean, 2002).

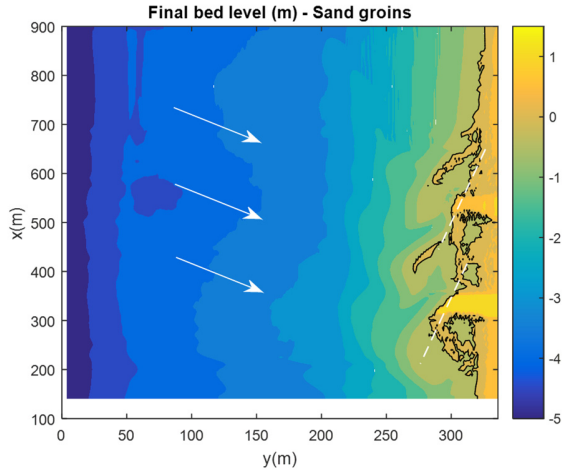

Fig. 12 Sand Groins: final numerical bathymetry

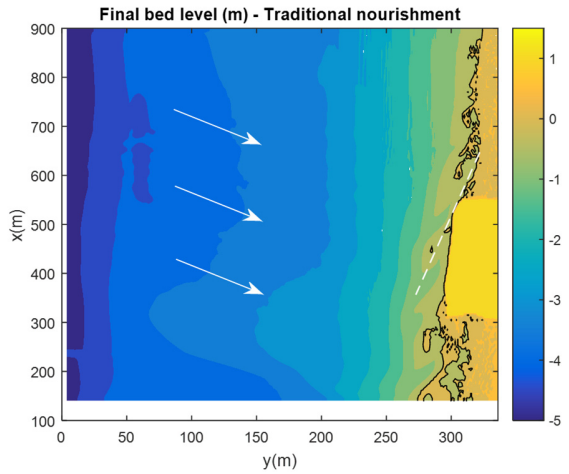

Fig. 13 Traditional nourishment: final numerical bathymetry

Fig. 14 shows the numerical volume accumulated in the updrift part of the nourishment, as in Fig. 11. Even if the simulated trend is similar to the observed one, the difference between traditional nourishment and sand groins is significantly larger than measured. This may be due to an important feature that the numerical model was unable to represent, probably the formation of a high steep bar at the shoreline (see Fig. 8 and Fig. 12).

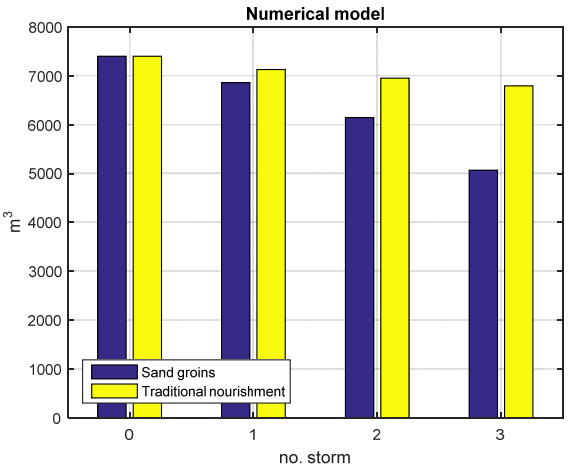

Fig. 14 Evolution of the volume of sand relative to the updrift half of the nourishment

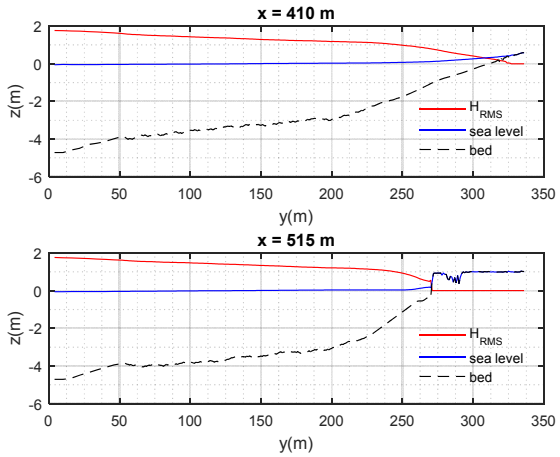

Fig. 15 Sand groins: wave height and sea level profile

Fig. 15 shows an example of the calculated set-up and the wave height along two profiles, one at the up-drift groin and one placed between the two sand groins, i.e. at longshore coordinates x = 515 m and x = 410 m, evaluated for t = 30 hours (during the first storm). The figure shows that the H_{RMS} wave height decreases smoothly along the profile due to wave breaking, experiencing an abrupt reduction at the groin head. The numerical tool is useful to describe the wave field, providing an accurate description that is difficult to achieve in the laboratory. In fact, the procedure to separate incident and reflected waves from the measured signals is affected by several uncertainties, as the mobile bed, the presence of a sloping bed, the presence of breaking waves, the strong-nonlinearity in shallow waters, the possible phase-locked reflection at the structures groin head.

The numerical simulation was very useful for interpreting the various ways the nourishment evolves, since it provided complete information on fluxes.

Fig. 16 shows the currents at t = 30 hours for the "sand groins" configuration with intensity in colour-scale. The currents are confined within a weaving narrow band that adheres to the shoreline. The largest values are predicted to be at the groin heads and directed slightly offshore. A small area, located up-stream of the first groin, is characterized by currents flowing against the main one. This return flow is responsible for developing the small ponds that characterized the "sand groins" profile.

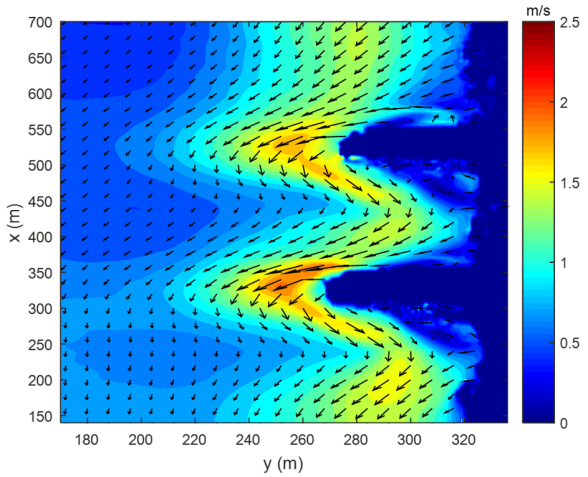

Fig. 16 Sand groins: currents

Fig. 17 shows the currents for the second configuration, with the same colour-scale used above. The currents have a slightly lower maximum intensity (~5%), with it being concentrated at the down-drift corner of the traditional nourishment.

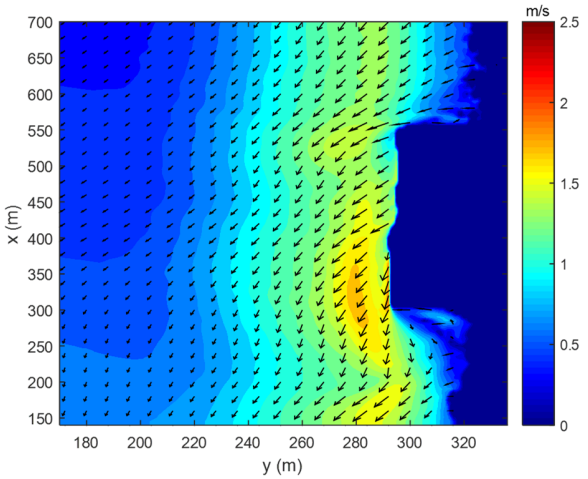

Fig. 17 Traditional nourishment: currents

The mean return flow due to mass flux and roller was included in the model and affected sediment transport, leading to offshore contribution. To balance this, effects of wave asymmetry and skewness were included, as well. However, since the implemented model was stationary (within each sea state), the non-stationary surf beat and the effects of the infragravity waves were not simulated.

Fig. 18 shows the long-shore and cross-shore sediment fluxes for the "sand groins" configuration (in colour-scale) as a result of the combined wave and current fields. Long-shore sediment transport was confined to a narrow region that widened slightly and intensified at the groin heads, and it is only just noticeable in the offshore zone. Cross-shore sediment transport was localized at the groin heads, with behaviour being almost symmetrical, although offshore contribution was larger than inshore contribution.

Fig. 19 shows a similar image for the second configuration using the same colour-scale. Long-shore sediment transport was concentrated in a wider area and dropped to zero in the offshore zone. Cross-shore sediment transport was very limited, with a local offshore peak at the up-stream corner of the nourishment.

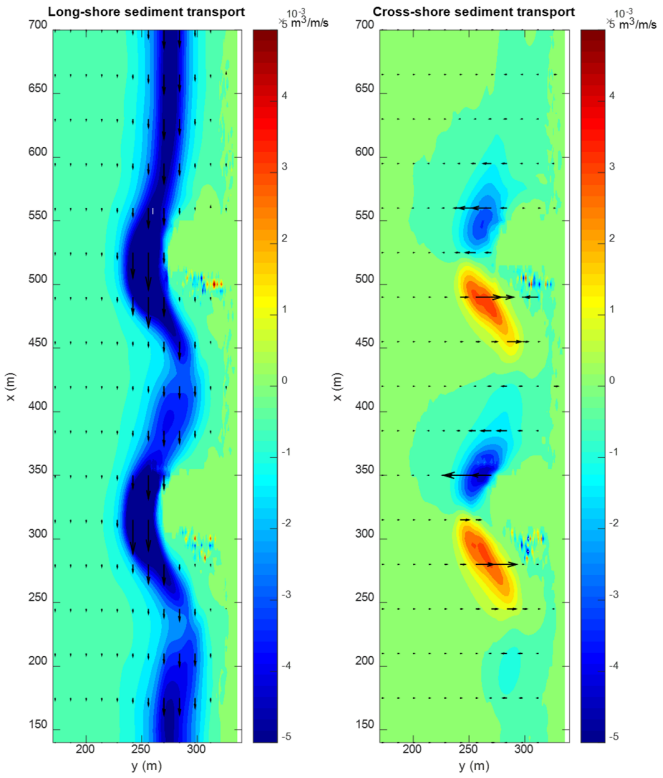

Fig. 18 Sand groins: long-shore (left) and cross-shore (right) sediment transport

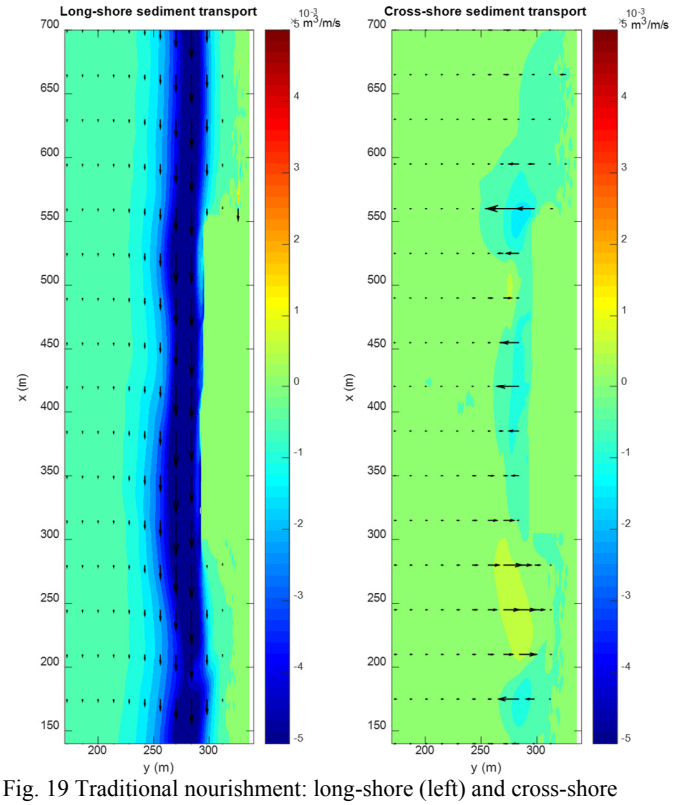

Fig. 19 Traditional nourishment: long-shore (left) and cross-shore (right) sediment transport

CONCLUSIONS

A combined experimental and numerical investigation was carried out in order to examine the evolution of two different types of small localized nourishment under the wave forcing of typical Italian storms, in view of possible application in the Northern Adriatic Sea.

Rectangular-shaped "traditional nourishment" was compared with an innovative "sand groin" layout, which is easier and more economical to build up.

Experiments were carried out in the University of Padova wave basin of the Department of Civil, Environmental and Architectural Engineering (ICEA), and the results are given in terms of bed evolution.

After three storms, the nourishment had been almost completely redistributed in both configurations, and the shoreline was almost completely aligned with the incident wave front.

The final shoreline in the "sand groins" configuration was shaped into an irregular beach line. In this case, stronger littoral currents and more active zones, in terms of sediment transport, as well as the formation of a small dune-lagoon system were observed. This behaviour can enhance biodiversity and it is also an interesting prospect for eco-tourism. However, the final beach shore-face created with traditional nourishment is probably more suited to traditional recreational beach use.

The calibration of the XBeach model against the experiments was provided. The calibrated numerical model predicted many of the observed features and proved to be a very useful tool for interpreting the hydro-morphodynamic processes associated with the short-term bed evolution analysed.

REFERENCES

De Winter, R. C., Gongriep, F., & Ruessink, B. G. (2015). Observations and modeling of alongshore variability in dune erosion at Egmond aan Zee, the Netherlands. *Coastal Eng.*, 99, 167-175.

Dean, R.G. (2002): Beach nourishment, theory and practice. Advanced Series on Ocean Engineering, 18, World Scientific, 399pp.

Dette, H. H., Larson, M., Murphy, J., Newe, J., Peters, K., Reniers, A., & Steetzel, H. (2002). Application of prototype flume tests for beach nourishment assessment. Coastal Engineering, 47(2), 137-177.

Dissanayake, P., Brown, J., Wisse, P., & Karunarathna, H. (2015). Effects of storm clustering on beach/dune evolution. *Marine Geology*, 370, 63-75.

Di Risio M., Lisi I., Beltrami G.M., De Girolamo P. (2010): Physical modeling of the cross-shore short-term evolution of protected and unprotected beach nourishments. *Ocean Eng.*, 37 (8–9), 777-789.

Grasso F., Michallet H., Barthélemy E. (2011): Experimental simulation of shoreface nourishments under storm events: A morphological, hydrodynamic, and sediment grain size analysis, *Coastal Eng.*, 58(2), 184-193.

Grüne J., Scmidt-Kopenhagen R., Wang Z. (2008): Cross-shore beach evolution large-scale laboratory tests with irregular waves, Proc. *Coastlab*, Bari, Italy

Harter, C., & Figlus, J. (2017). Numerical modeling of the morphodynamic response of a low-lying barrier island beach and foredune system inundated during Hurricane Ike using XBeach and CSHORE. *Coastal Engineering*, 120, 64-74.

Janssen, T. T., & Battjes, J. A. (2007). A note on wave energy dissipation over steep beaches. *Coastal Eng.*, 54(9), 711-716.

Karasu, S., Work, P. A., Cambazoğlu, M. K., & Yüksek, Ö. (2008). Coupled longshore and cross-shore models for beach nourishment evolution at laboratory scale. Journal of waterway, port, coastal, and ocean engineering, 134(1), 30-39.

Kobayashi, N. (2016) Coastal Sediment Transport Modeling for Engineering Applications. *Journal of Waterway, Port, Coastal, and Ocean Engineering* 142:6.

Martinelli, L., Zanuttigh, B., & Lamberti, A. (2006). Hydrodynamic and morphodynamic response of isolated and multiple low crested structures: Experiments and simulations. *Coastal Eng.*, 53(4), 363-379.

McCall, R. T., De Vries, J. V. T., Plant, N. G., Van Dongeren, A. R., Roelvink, J. A., Thompson, D. M., & Reniers, A. J. H. M. (2010). Two-dimensional time dependent hurricane overwash and erosion modeling at Santa Rosa Island. *Coastal Eng.*, 57(7), 668-683.

Nash, J.E., Sutcliffe, J.V., (1970). River flow forecasting through conceptual models. *J. Hydrol*. 10, 282–290.

Roelvink, D., Reniers, A., Van Dongeren, A. P., de Vries, J. V. T., McCall, R., & Lescinski, J. (2009). Modelling storm impacts on beaches, dunes and barrier islands. *Coastal Eng.*, 56(11), 1133-1152.

Ruessink B.G., Blenkinsopp C., Brinkkemper J.A., Castelle B., Dubarbier B., Grasso F., Puleo J.A., Lanckriet T. (2016): Sandbar and beach-face evolution on a prototype coarse sandy barrier, *Coastal Eng.*, 113, 19-32.

Ruol P., Capobianco M., Tondello M. (1997): Physical model tests in the frameworks of beach nourishment performance evaluation. *MEDCOAST* Kawra, Malta.

Ruol, P., Martinelli, L., Favaretto, C. (2018). Vulnerability analysis of the Venetian littoral and adopted mitigation strategy. *Water*, 10(8), 984.

Simmons, J. A., Splinter, K. D., Harley, M. D., & Turner, I. L. (2019). Calibration data requirements for modelling subaerial beach storm erosion. *Coastal Engineering*, 152, 103507

Soulsby, R. L. (1997). Dynamics of Marine Sands Thomas Telford Publications. London, UK.

Stive M, de Schipper M., Luijendijk A., Aarninkhof S., van Gelder-Maas C., de Vries J., de Vries S., Henriquez M., Marx S., and Ranasinghe R. (2013): A New Alternative to Saving Our Beaches from Sea-Level Rise: The Sand Engine. *J. of Coastal Res.*, 29 (5), 1001 – 1008.

Tondello, M., Ruol, P., Sclavo, M., & Capobianco, M. (1999). Model Tests for Evaluating Beach Nourishment Performance. *In Coastal Engineering Proceedings* 1998 (pp. 3096-3109).

Van Gent, M. R. A., de Vries, J. V. T., Coeveld, E. M., De Vroeg, J. H., & Van de Graaff, J. (2008). Large-scale dune erosion tests to study the influence of wave periods. *Coastal Eng.*, 55(12), 1041-1051.

Van Rijn, L. C. (1984). Sediment transport, part III: bed forms and alluvial roughness. *Journal of hydraulic Eng.*, 110(12), 1733-1754.

Van Thiel de Vries, J. S. M. (2009). Dune erosion during storm surges. (Ph.D. dissertation), Delft University of Technology, Delft, 2009.

Williams, J. J., Esteves, L. S., & Rochford, L. A. (2015). Modelling storm responses on a high-energy coastline with XBeach. *Modeling Earth Systems and Environment*, 1(1-2), 3.

Wilmott, C.J., Ackleson, S.G, Davis, E., Feddema, J., Klink, M., Legates, D.R., O'Donnell, J., Rowe, M.C. (1985). Statistics for the evaluation and comparison of models. *J. Geophys. Res*. 90, 8995–9005.

Work, P. A., & Rogers, W. E. (1998). Laboratory study of beach nourishment behavior. Journal of waterway, port, coastal, and ocean engineering, 124(5), 229-237.

ANNEX: EVALUATION OF MODEL PERFORMANCE

The following performance indexes were used to check the agreement between modelled (P_i) and experimental (O_i) results:

1) the Nash-Sutcliff efficiency NSE (Nash and Sutcliffe, 1970),

$$NSE = 1 - \frac{\sum_i (O_i - P_i)^2}{\sum_i (O_i - \langle O_i \rangle)^2} \quad (1)$$

2) the index of agreement D proposed by Wilmott (1985).

$$D = 1 - \frac{\sum_i (P_i - O_i)^2}{\sum_i (|P_i - \langle O_i \rangle| + |O_i - \langle O_i \rangle|)^2} \quad (2)$$

Perfect agreement is achieved when D and NSE are equal to unity.

Tab. A.1 Sand groins: variables value analyzed

-	beta	wetslp	z0	hswitch	dzmax
beta	0.050	0.06	0.02	0.55	0.05
beta	0.055	0.06	0.02	0.55	0.05
beta	0.060	0.06	0.02	0.55	0.05
beta	0.110	0.06	0.02	0.55	0.05
wetslp	0.06	0.045	0.02	0.55	0.05
wetslp	0.06	0.05	0.02	0.55	0.05
wetslp	0.06	0.055	0.02	0.55	0.05
wetslp	0.06	0.06	0.02	0.55	0.05
wetslp	0.06	0.065	0.02	0.55	0.05
wetslp	0.06	0.07	0.02	0.55	0.05
z0	0.06	0.055	0.006	0.55	0.05
z0	0.06	0.055	0.011	0.55	0.05
z0	0.06	0.055	0.02	0.55	0.05
z0	0.06	0.055	0.025	0.55	0.05
z0	0.06	0.055	0.03	0.55	0.05
hswitch	0.06	0.055	0.02	0.35	0.05
hswitch	0.06	0.055	0.02	0.45	0.05
hswitch	0.06	0.055	0.02	0.55	0.05
hswitch	0.06	0.055	0.02	0.65	0.05
hswitch	0.06	0.055	0.02	0.75	0.05
dzmax	0.06	0.055	0.02	0.55	0.03
dzmax	0.06	0.055	0.02	0.55	0.05
dzmax	0.06	0.055	0.02	0.55	0.09
dzmax	0.06	0.055	0.02	0.55	0.2
dzmax	0.06	0.055	0.02	0.55	0.4
dzmax	0.06	0.055	0.02	0.55	0.6

Tab. A.2 Sand groins: Beta calibration – NSE index

beta	after 1st storm	after 2nd storm	after 3rd storm	average NSE
0.050	0.717	0.492	0.492	0.566
0.055	0.737	0.557	0.500	0.598
0.060	0.817	0.726	0.526	0.690
0.110	0.811	0.732	0.418	0.653

Tab. A.3 Sand groins: Beta calibration – D index

beta	after 1st storm	after 2nd storm	after 3rd storm	average D
0.050	0.917	0.852	0.833	0.867
0.055	0.926	0.875	0.838	0.880
0.060	0.947	0.922	0.861	0.910
0.110	0.946	0.921	0.805	0.890

Tab. A.4 Sand groins: Wetslp calibration – NSE index

wetslp	after 1st storm	after 2nd storm	after 3rd storm	average NSE
0.045	0.821	0.640	0.599	0.687
0.050	0.815	0.624	0.620	0.686
0.055	0.815	0.636	0.635	0.695
0.060	0.814	0.606	0.610	0.677
0.065	0.807	0.595	0.595	0.666
0.070	0.799	0.586	0.574	0.653

Tab. A.5 Sand groins: Wetslp calibration – D index

wetslp	after 1st storm	after 2nd storm	after 3rd storm	average D
0.045	0.955	0.909	0.886	0.917
0.050	0.954	0.906	0.890	0.917
0.055	0.954	0.908	0.894	0.919
0.060	0.955	0.904	0.890	0.916
0.065	0.953	0.901	0.882	0.912
0.070	0.951	0.898	0.875	0.908

Tab. A.6 Sand groins: z0 calibration – NSE index

z0	after 1st storm	after 2nd storm	after 3rd storm	average NSE
0.006	0.754	0.577	0.508	0.613
0.011	0.813	0.607	0.613	0.678
0.020	0.815	0.636	0.635	0.695
0.025	0.806	0.606	0.554	0.655
0.030	0.799	0.595	0.486	0.627

Tab. A.7 Sand groins: z0 calibration – D index

z0	after 1st storm	after 2nd storm	after 3rd storm	average D
0.006	0.934	0.894	0.861	0.896
0.011	0.952	0.813	0.894	0.886
0.020	0.954	0.908	0.894	0.919
0.025	0.953	0.906	0.872	0.910
0.030	0.951	0.902	0.853	0.902

Tab. A.8 Sand groins: hswitch calibration – NSE index

hswitch	after 1st storm	after 2nd storm	after 3rd storm	average NSE
0.35	0.805	0.572	0.559	0.646
0.45	0.804	0.595	0.586	0.662
0.55	0.815	0.636	0.635	0.695
0.65	0.812	0.618	0.611	0.681
0.75	0.807	0.607	0.560	0.658

Tab. A.9 Sand groins: hswitch calibration – D index

hswitc:	after 1st storm	after 2nd storm	after 3rd storm	average D
0.35	0.948	0.885	0.866	0.900
0.45	0.951	0.898	0.879	0.909
0.55	0.954	0.908	0.894	0.919
0.65	0.956	0.908	0.893	0.919
0.75	0.955	0.907	0.881	0.914

Tab. A.10 Sand groins: dzmax calibration – NSE index

dzmax	after 1st storm	after 2nd storm	after 3rd storm	average NSE
0.03	0.825	0.648	0.646	0.706
0.05	0.815	0.636	0.635	0.695
0.09	0.816	0.621	0.619	0.685
0.20	0.802	0.593	0.625	0.673
0.40	0.812	0.604	0.609	0.675
0.60	0.818	0.610	0.583	0.670

Tab. A.11 Sand groins: dzmax calibration – D index

dzmax	after 1st storm	after 2nd storm	after 3rd storm	average D
0.03	0.957	0.911	0.898	0.922
0.05	0.954	0.908	0.894	0.919
0.09	0.954	0.904	0.889	0.916
0.20	0.951	0.898	0.895	0.915
0.40	0.952	0.897	0.885	0.911
0.60	0.953	0.898	0.874	0.908

Tab. B.1 Traditional nourishment: variables value analyzed

-	beta	wetslp	z0	hswitch	tsfac
beta	0.065	0.6	0.02	0.55	0.089
beta	0.085	0.6	0.02	0.55	0.089
beta	0.095	0.6	0.02	0.55	0.089
beta	0.1	0.6	0.02	0.55	0.089
beta	0.11	0.6	0.02	0.55	0.089
wetslp	0.095	0.045	0.02	0.55	0.089
wetslp	0.095	0.05	0.02	0.55	0.089
wetslp	0.095	0.055	0.02	0.55	0.089
wetslp	0.095	0.06	0.02	0.55	0.089
wetslp	0.095	0.065	0.02	0.55	0.089
wetslp	0.095	0.07	0.02	0.55	0.089
z0	0.095	0.06	0.0095	0.55	0.089
z0	0.095	0.06	0.011	0.55	0.089
z0	0.095	0.06	0.015	0.55	0.089
z0	0.095	0.06	0.019	0.55	0.089
z0	0.095	0.06	0.023	0.55	0.089
hswitch	0.095	0.06	0.015	0.25	0.089
hswitch	0.095	0.06	0.015	0.5	0.089
hswitch	0.095	0.06	0.015	0.55	0.089
hswitch	0.095	0.06	0.015	0.6	0.089
hswitch	0.095	0.06	0.015	0.8	0.089
tsfac	0.095	0.06	0.015	0.55	0.01
tsfac	0.095	0.06	0.015	0.55	0.03
tsfac	0.095	0.06	0.015	0.55	0.06
tsfac	0.095	0.06	0.015	0.55	0.089
tsfac	0.095	0.06	0.015	0.55	0.12

Tab. B.2 Traditional nourishment: Beta calibration – NSE index

beta	after 1st storm	after 2nd storm	after 3rd storm	average NSE
0.065	0.900	0.825	0.699	0.808
0.085	0.938	0.855	0.774	0.856
0.095	0.943	0.847	0.785	0.859
0.100	0.944	0.848	0.777	0.856
0.110	0.939	0.842	0.760	0.847

Tab. B.3 Traditional nourishment: Beta calibration – D index

beta	after 1st storm	after 2nd storm	after 3rd storm	average D
0.065	0.972	0.947	0.910	0.943
0.085	0.983	0.957	0.933	0.958
0.095	0.984	0.955	0.938	0.959
0.100	0.984	0.954	0.934	0.958
0.110	0.983	0.953	0.930	0.956

Tab. B.4 Traditional nourishment: Wetslp calibration – NSE index

wetslp	after 1st storm	after 2nd storm	after 3rd storm	average NSE
0.045	0.938	0.847	0.747	0.844
0.050	0.939	0.844	0.771	0.851
0.055	0.931	0.841	0.769	0.847
0.060	0.943	0.847	0.785	0.859
0.065	0.942	0.849	0.774	0.855
0.070	0.943	0.847	0.775	0.855

Tab. B.5 Traditional nourishment: Wetslp calibration – D index

wetslp	after 1st storm	after 2nd storm	after 3rd storm	average D
0.045	0.982	0.953	0.923	0.953
0.050	0.983	0.954	0.934	0.957
0.055	0.981	0.954	0.934	0.956
0.060	0.984	0.955	0.938	0.959
0.065	0.984	0.956	0.934	0.958
0.070	0.984	0.954	0.932	0.957

Tab. B.6 Traditional nourishment: z0 calibration – NSE index

z0	after 1st storm	after 2nd storm	after 3rd storm	average NSE
0.010	0.926	0.861	0.766	0.851
0.011	0.929	0.857	0.788	0.858
0.015	0.938	0.874	0.770	0.861
0.019	0.935	0.851	0.779	0.855
0.023	0.940	0.841	0.779	0.853

Tab. B.7 Traditional nourishment: z0 calibration – D index

z0:	after 1st storm	after 2nd storm	after 3rd storm	average D
0.010	0.978	0.959	0.933	0.957
0.011	0.980	0.958	0.939	0.959
0.015	0.983	0.963	0.933	0.960
0.019	0.982	0.957	0.936	0.958
0.023	0.983	0.952	0.935	0.957

Tab. B.8 Traditional nourishment: hswitch calibration – NSE index

hswitch	after 1st storm	after 2nd storm	after 3rd storm	average NSE
0.250	0.924	0.829	0.758	0.837
0.500	0.932	0.854	0.735	0.840
0.550	0.938	0.874	0.770	0.861
0.600	0.927	0.844	0.774	0.849
0.800	0.934	0.847	0.764	0.849

Tab. B.9 Traditional nourishment: hswitch calibration – D index

hswitch:	after 1st storm	after 2nd storm	after 3rd storm	average D
0.250	0.978	0.947	0.926	0.950
0.500	0.981	0.957	0.922	0.953
0.550	0.983	0.963	0.933	0.960
0.600	0.980	0.955	0.935	0.956
0.800	0.981	0.956	0.933	0.957

Tab. B.10 Traditional nourishment: tsfac calibration – NSE index

tsfac	after 1st storm	after 2nd storm	after 3rd storm	average NSE
0.010	0.925	0.855	0.768	0.849
0.030	0.918	0.885	0.780	0.849
0.060	0.933	0.841	0.758	0.844
0.089	0.938	0.874	0.770	0.861
0.120	0.933	0.857	0.784	0.858

Tab. B.11 Traditional nourishment: tsfac calibration – D index

tsfac	after 1st storm	after 2nd storm	after 3rd storm	average D
0.010	0.979	0.958	0.933	0.956
0.030	0.977	0.956	0.936	0.957
0.060	0.981	0.953	0.929	0.954
0.089	0.983	0.963	0.933	0.960
0.120	0.981	0.958	0.938	0.959